Combining ionic diode, resistive pulse and membrane for detection and separation of anti-CD44 antibody

Imad Abrao-Nemeir, Oumaima Zaki, Nathan Meyer, Mathilde Lepoitevin, Joan Torrent, Jean-Marc Janot, Sebastien Balme

Combining ionic diode, resistive pulse and membrane for detection and separation of anti-CD44 antibody.

Imad Abrao-Neimer[a], Oumaima Zaki[a], Nathan Meyer[a,b], Mathilde Lepoitevin[c], Joan Torrent[b], Jean-Marc Janot[a], Sebastien Balme*[a]

[a] Institut Européen des Membranes, UMR5635 University of Montpellier ENCSM CNRS, Place Eugène Bataillon, 34095 Montpellier cedex 5, France.

[b] INM, University of Montpellier , INSERM, Montpellier, France

[c] Institut des Matériaux Poreux de Paris (IMAP), UMR 8004 CNRS, Ecole Normale Supérieure de Paris, Ecole Supérieure de Physique et de Chimie Industrielles de Paris, PSL Université, 75005 Paris, France

Abstract

The need for antibody protein is growing for both diagnosis and therapy. In this work, we combine two strategies based on single nanopore sensing and multipore membrane to separate, detect and identify antibodies. This proof of concept was done for the anti-CD44. In a first step, a single nanopore with a bullet shape were designed using track-etching of polymer film and functionalized, with a PEG spacer and CD44 antigen. The detection of anti-CD44 was evidenced by an inversion of the current rectification. After demonstrating the ability to specifically detect the antiCD44 in a single nanopore, a multipore membrane with cylindrical nanopore was designed following the same protocol and used to elute a solution of anti-CD44.In a second step, the elution product was analysed using a single SiN nanopore showing that the anti-CD44 and CD44 antigen are extracted from the membrane. The analysis of the amplitude of the current blockade shows that the complex is dissociated.

1. Introduction

The increasing need for the identification of proteins as biomarkers as well as their synthesis as therapeutic agents requires the development of innovative solutions for their analysis, production and identification [1,2]. The protein extraction from complex biological matrices is usually done using numerous methods including dialysis, centrifugation, electrophoresis, chromatography, 2D

gel or immunoprecipitation [3–5]. More recently, microfluidic techniques met a great interest because of the possibility of multiplexing channels and low volume required (10^{-9} to 10^{-18} L) [6,7]. This interest is emphasized by proteomic advances. They require that the separation is connected to a detector with a high sensitivity, providing information about the presence of the target protein [8]. Membrane chromatography for protein separation has emerged several decades ago for analysis [9,10] and more recently for production [11–14]. However, they stayed as a concept for protein analysis due to numerous bottlenecks such as low surface volume ratio, limiting the quantity of protein bonding [15,16]. This makes impossible to detect the eluted analyte directly from the membrane to common detection devices.

On the other hand, the sensing technology based on single polymers and solid-state nanopore has demonstrated numerous achievements in the area of protein detection, discrimination, and identification of assembly [17]. There are basically two ways to detect protein using such nanopore. The first one is based on ionic diode properties [18,19]. Such properties are usually obtained in asymmetrical (conical or bullet-like shape) nanopore made in polymer film using track-etching technique [20–23]. Because of the asymmetrical shape and the surface charge, the current-voltage (I-V) response is not linear [24–26]. Thus, when the target binds to the probe grafted inside the nanopore, it induces a modification of inner surface wall properties that is immediately followed by a modification of the ionic transport generating a change in the ionic diode signal [27,28]. This type of nanopore was previously used to detect several proteins such as lysozyme [29–34], antibodies[35], and biopolymers [36]. Despite the possibility to specifically detect a target, the ionic diode is not suitable for a fine characterization of proteins or provide information on their possible structural modification [17]. To do so, a second way can be used involving resistive pulse sensing (RPS) [37,38]. The RPS consists of applying a constant voltage through a single nanopore and record the ionic current. The passage to an analyte induces a

current perturbation characterized by an amplitude and duration. The resistive pulse has already been used for protein or antibody analysis [39–43]. The current perturbations provide a fingerprint of the protein or protein assembly [44–52]. The RPS sensing can be done at protein concentrations in the nM range and does not require labelling. This technique is also gaining interest since the development of dielectric breakdown manufacturing that allows single nanopore fabrication, making it more accessible than electrons or ions beam that require expensive facilities [53,54].

Combining these different single nanopore and classical membrane approaches could be an interesting way to detect, separate and characterize a protein with minimum steps and a go/no-go information during the separation step. It is interesting to note that the investigations combining single and multipore membranes mainly deal with osmotic energy production. This combined approach provides a fundamental understanding of ionic transport at the single nanopore scale and evaluation of the efficiency on multipore membranes [55,56]. Conceptually for proteins, the separation and detection steps will involve the use of a track-etched membrane that is scalable from a single nanopore membrane and high density of nanopore membrane (10^5 to 10^{11} pores/cm^2). Placed in paralleled, the single nanopore membrane "sensor" validate whether the analyte is present in the solution while multipore the membrane separates the analyte from the matrix. These two singles and multipore membranes can be produced and functionalized with a probe following exactly the same conditions [23,57], and thus the sensor have the same physico-chemical properties as separation membrane. In the second step, the target protein separated by the multipore membrane will be analysed using a single SiN nanopore by resistive pulse sensing.

Here, we demonstrate a new approach combining different single and multi-pore membrane technologies for separation, detection and analysis of antibodies. We selected the CD44 antigen

(AgCD44) and its associated antibodies (anti-CD44) due to their involvement in cancer [58] or as a monoclonal antibody-based therapeutic agent [59]. For this purpose, single pores are produced by track etching method and functionalized with AgCD44 as probe. Then, we demonstrate that the AgCD44 grafting does not alter its specificity to detect anti-CD44 before producing multipore membranes under the same conditions to selectively capture anti-CD44. In a second step, the complex anti-CD44/AgCD44 is eluted from the multipore membrane and analysed by a single SiN nanopore using the resistive pulse method. This second step will aim to demonstrate if the elution process maintains the complex AgCD44/anti-CD44.

2. Materials and Method

2.1. Materials

The 13 µm thick PET films with biaxial orientations were purchased from Goodfellow (ES301130). EDC (≥99.0%, 03449), HCl (30721) NaOH (≥98%, 30620), MES (≥99.5%, M8250), NaCl (≥99.5% , S7653), Ethylenediamine (≥99%, E26266), $NiCl_2$ (98%, 339350), ethylenediaminetetraacetic acid (EDTA) (98.5-101.5%, E5513), CD44 Antigen (APREST83079), BSA (A9418), lysozyme (05281), Avidin (A9275), Anti-avidin (B9655), Anti-BSA (SAB4301142), L-DOPA (≥98%, D9629) and PBS tab buffer (P4417) were purchased from Sigma-Aldrich. NHS-PEG-NTA (228PG2-NSNT-2K) were purchased from Nanocs. KCl (≥ 99.5%, POCL-00A) was purchased from Labkem. Dowfax 2A1 (lot #TO20884587-02) was purchased from EZkem. CD44 antibody (ANT-242) was purchased from PROSPEC.

2.2. Membrane design

2.2.1. Single and multipore track-etched membrane

The 13 µm thick PET films were irradiated by heavy swift ion Kr (9 MeV) at GANIL (Caen, France). The single pores were obtained from a single track while the multipore membranes were obtained with a fluency of 10^8 ion/cm^2[55] . To obtain a bullet-shaped nanopore (single and multipore membranes), only one side of the film was exposed to UV at 312 nm for 26 hours avoiding surfactant adsorption[60,61]. The chemical etching was done using a solution containing 6 M NaOH and 0.05% Dowfax, heated at 60°C for 6 min. Then, the pore was rinsed with ultrapure water into successive baths of 10 min, 15 min, 30 min, one hour and then overnight.. To obtain cylindrical nanopore (multipore membrane only), the irradiated polymer films were activated by 12 h per side exposition to UV at 312 nm[62]. Then the chemical etching was done under NaOH 4M solution at 40°C for 4 min to obtain nanopore with a diameter around 100 nm.

2.2.2. Track-etched nanopore and membrane functionalization

Single and multipore PET membrane were functionalized using the same procedure. The membrane (single or multipore) was immersed overnight in a solution of ethylenediamine (1:100) in MES buffer 0.1 M containing 0.05 M of EDC (pH was adjusted to 4.5 ± 0.5 with HCl) [63]. Then, a small amount of NHS-PEG-NTA was added to 1 mL of PBS for 12 hours. The membranes (single and multipore) were then rinsed by Milli-Q water and incubated in a BSA solution at 1 mg/mL for 3 hours. Next, $NiCl_2$ solution 100 mM was added for 1 hour. Finally, CD44 antigen His-tag was added to the tip side of the nanopore and incubated for 3 hours. This was followed by incubation of the membrane with three different anti-CD44 (3 µg/mL) for 1 hour each. The washing solution was prepared with 500 mM imidazole and 100 mM EDTA, the pH was adjusted to 8.

2.3. Ionic diode measurement

The current-voltage (I-V) measurements were performed with an eONE XV amplifier. The current was measured by Ag/AgCl electrodes. One electrode is connected to the working electrode the

amplifier and the second one is connected to the ground. The working electrode and the ground were place on the tip and the base side of nanopore respectively (Figure 1e). The I-V curves were recorded using PBS solution 1X after each step of the functionalization and antibody detection.

2.4. Filtration

For the filtration, 1.3 cm diameter multipore membranes (pore density 10^8 pore/cm^2) were functionalized and then placed into a filtration system made of Teflon (r= 0.6 cm) into which the sample is injected via a syringe. The filtration process was done using Harvard apparatus PHD 2000 perfusion, and consists of three steps: first, the passage of 250 µL of the anti-CD44 (3.37 µg/mL) at a flow rate of 167 µL/h. Next, the membrane was washed with PBS before to remove any molecules not bound to the immobilized receptors. Finally, 250 µL of the washing solution was passed through at a flow rate of 167 µL/hr to remove the complex AgCD44/Anti-CD44.

2.5. Resistive pulse sensing

2.5.1. SiN drilling and coating

The single nanopore was drilled inside stressless SiN, 12 nm thick (Norcada) by dielectric breakdown using Northern Nanopore instruments. Briefly, the SiN film was washed in piranha (H_2SO_4:H_20_2, 3:1) solution at 90°C for 1 hour. Then, it was rinsed with Milli-Q water and dried thoroughly using an air gun, before being placed in the microfluidic cell (Northern Nanopore). The system was then flushed with 600 µL of propan-2-ol before being filled with deionized and degassed water. After that, the cell was filled with a solution of KCl (1 M)/ HEPES (8.3 mM), the pH is then adjusted to 8 by KOH (1 M). Then a potential ramp from 0 to 5 V followed by a slower ramp from 5 to 14 V was applied across the microchip until a pore opening is detected. Once the

nanopore is formed, the solution was changed to NaCl 1.5 M, HEPES 8.3 mM at pH 8 (adjusted using NaOH 1 M) for the conditioning step. The latter consists to apply a voltage box from -3 V to 3 V for several cycles until the nanopore reached the desired diameter, here about 9.5 nm. After nanopore opening and characterization by measurement of the conductance, the nanopore was incubated with saturated L-DOPA (c = 10µg/ml) solution in degassed deionized water for 2 hours. Then the current was measured for 1 min using -300 mV and +300 mV in order to assess the noise level of the nanopore.

2.5.2. Protein detection and analysis

Protein detection through SiN nanopore (diameter about 9.5 nm) was performed by resistive pulse using electrolyte solution NaCl 2 M, PBS 1X, pH 7.4. The solution of AgCD44, anti-CD44 and complex AgCD44/anti-CD44 use for calibration was prepared at 20 nM. The protein solution was placed on the half-cell connected to the working electrode, the ground was placed on the opposite side (figure 1) then applying a voltage of -300 mV for 5 min for each protein solution. The ionic current was recorded at sampling rate 200 kHz with a Bessel filter at 10 kHz. The data acquisition was performed with a HEKA EPC800 amplifier coupled with a LIH 8+8 acquisition card using patchmaster software (HEKA electronics, Germany). The current drop induced by the proteins were detected using a custom-made LabVIEW software “Peak Nano Tools”. The current traces were filtered at 5 kHz with a Butterworth filter. The threshold for event detection was determined as 6 times the standard deviation after correction of baseline fluctuations by a Savitzky−Golay filter. The current drop call events were characterized by a dwell time, and an amplitude of the blockade of the current as $\Delta I/I_0$.

Fluorescence measurement

The fluorescence correlation spectroscopy was performed using lab-made confocal spectrometer previously described [42]. Anti-CD44 was labelled with the alexa-fluor 640 under buffer NaCl 500 mM, Tris 5 mM, pH 7.5 at a concentration around 1 nM.

3. Results and discussion

3.1. Track etched design and functionalization

Single and multipore nanopore membranes were obtained by the track-etched technique on PET films (13 µm) To obtain the sensors, we designed a single asymmetric nanopore for their ionic diode properties. To this end, bullet-like shape nanopore was achieved by the addition of Dowfax 2:1 surfactant in the etching solution thanks to the different etching rate due to the exposure or not of the PET surface to UV light [64] (Figure 1e). The diameters d_{tip} and D_{base} were determined by scanning electron microscopy (SEM) on multipore membranes with high pore density obtained under the same conditions (Figure 1a-b). For an etching time of 6 minutes at a temperature of 60 °C, the histogram of measured d_{tip} and D_{base} are centred at 130 +/- 20 nm and 320 +/- 50 nm respectively (Figure 1c-d). Because it exists variability in nanopore size, each single nanopore was characterized by ionic conductance measurements. After the chemical etching, the I-V curves recorded in PBS 1X are non-linear due to the negative charge of the carboxylate moieties. The origin of this current rectification is the non-homogeneous distribution of ions along the nanopore as previously reported[65,66] . It depends on the electrolyte concentration and the nanopore shape and surface charge. Thereby, a weak modification of the nanopore surface state due to a functionalization step or the binding of an analyte induce a modification of I-V curve shape that can be characterized by a change of the rectification factor (eq 1)

$$R_f = \log\left|{I_{(+1.5V)}}/{I_{(-1.5V)}}\right| \quad (1)$$

Under our conditions, a positive value of R_f reflects a global negative charge of the nanopore surface. On the contrary, an inversion of R_f toward negative values is induced by a global positive surface charge of the nanopore. The functionalization of the single nanopore requires 4 steps (Figure 2a) before binding the AgCD44. Due to the variability of the nanopore, the rectification factors are given by the average value and the error bars correspond to the standard errors obtained on 8 independent single nanopores. For each I-V curve, at least 10 measurements were performed and averaged. The first functionalization step consists of adding ethylenediamine to the carboxylate moieties. The success of this step is evidenced by a decrease or an inversion of the R_f value due to a partial conversion of the COO^- of the PET by positive charges of the NH_3^+ moieties. In the second step, the NHS-PEG-NTA is grafted in the presence of EDC. We observe that the current rectification increases due to the replacing of NH_3^+ moieties by negative charge of carboxylate moieties of PET-NTA. This confirms that the functionalization was successful. The next steps consist of the addition of the AgCD44 with a histidine tag after addition of Ni^{2+}. It is obvious that the addition of PEG as a spacer will not avoid the non-specific adsorption of AgCD44. Indeed, the reported density for carboxylic groups inside a PET nanopore is about 0.2 COOH/nm^2 [67]. In addition, the successive functionalization steps do not have a 100 % yield. Considering that, there are spaces between the PEG-NTA chains where the AgCD44 can be adsorbed. This could lead to a modification of the nanopore surface and thus play a role in the R_f value.

There are several strategies to reduce non-specific adsorption [68]. The most effective is high density PEG grafting. This option is not suitable as it is limited to the number of grafting points in the nanopore, in our case, that would be the carboxylate moieties' density. Another solution is to adsorb BSA in the free spaces. We used this second strategy. After adsorption of BSA on the nanopore using a solution at 1 mg/mL in PBS, we notice a decrease in the R_f. This confirms the presence of free space between the PEG-NTA. We determined an optimal incubation time of 3

hours as after the measured rectification factor stays constant. Once BSA was adsorbed, Ni^{2+} was added for 3h. The chelation of Ni^{2+} on the carboxylate moieties and tertiary amine of NTA functions induces an inversion of the rectification factor due to an addition of positive charge in the nanopore. We notice that the values of the current and the thus the R_f are not strictly identical for all the single nanopores. This is due to the variability in the size of the nanopore and the functionalization rates. However, the trends are identical regardless the nanopore.

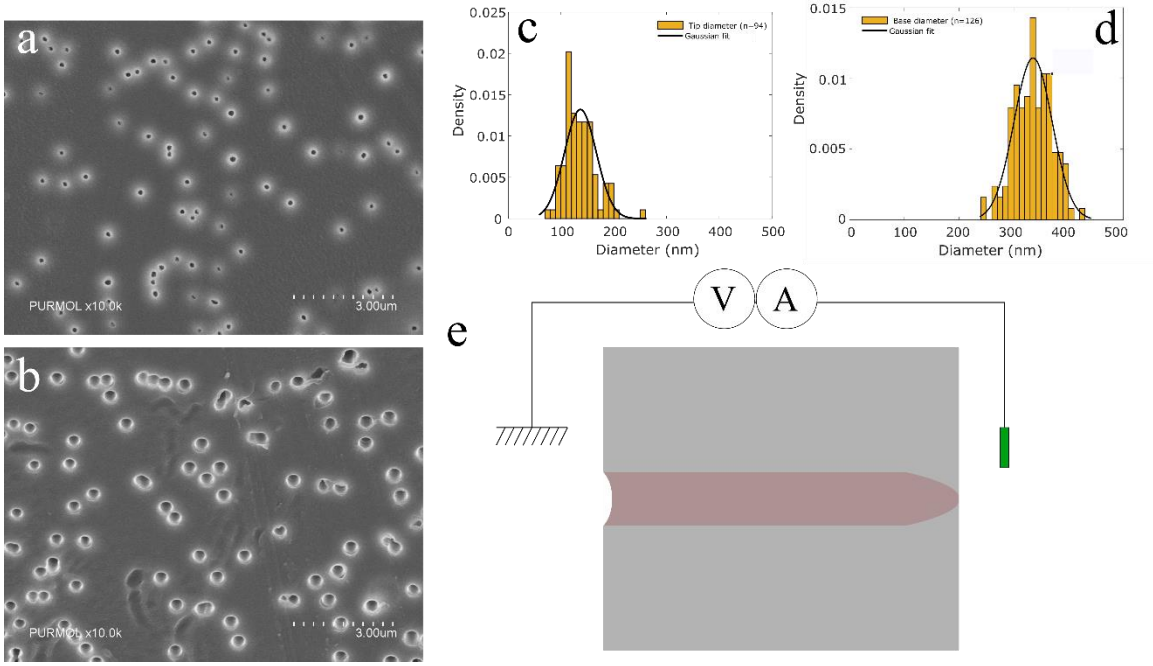

Figure 1 : SEM of bullet shape multipore membrane open under the same condition that single nanopore. (a) is the tip side and (b) the base and the associate histogram of diameter (c) and (d) respectively. (e) Scheme of single bullet shape nanopore for the measurement of the current of the ionic diode under an applied potential.

3.2. Anti-CD44 detection

Our aim is to detect the anti-CD44. For this, the probe selected is the AgCD44 with a histidine-tag because the two amines of imidazole moieties specifically chelate the Ni^{2+} loaded on the PEG-NTA grafted inside the nanopore. The nanopore incubates for 3 hours in the AgCD44-his-tag solution

and then the I-V curves are recorded. We observe an inversion of the R_f which is in good agreement with a negative global charge of the AgCD44 at pH 7.2 (IEP 4.9 calculated from IPC). We therefore attempted to detect the anti-CD44 in PBS solution at a concentration of 3 µg/ml. After incubation for 90 min, the R_f reverses toward negative values. We note at this point that the successive inversion of the R_f recorded after the Ni^{+2} addition, AgCD44 and antiCD44 occurred on all single nanopores (n=8). This allows, despite the variability of the *Rf* values inherent to the distribution of single nanopore size (as shown for multipore membrane on figure 1), to control of the last steps of the functionalization and the detection of the antibody. We rinsed the nanopore with an imidazole solution that contains EDTA In order to release the AgCD44/anti-CD44 complex. After washing, the rectification reverses to reach a range close to the step before the addition of Ni^{2+} suggesting that the complex is filtrated. However, this will be confirmed later by experiments using multipore membranes and further analysis of the filtrate solution.

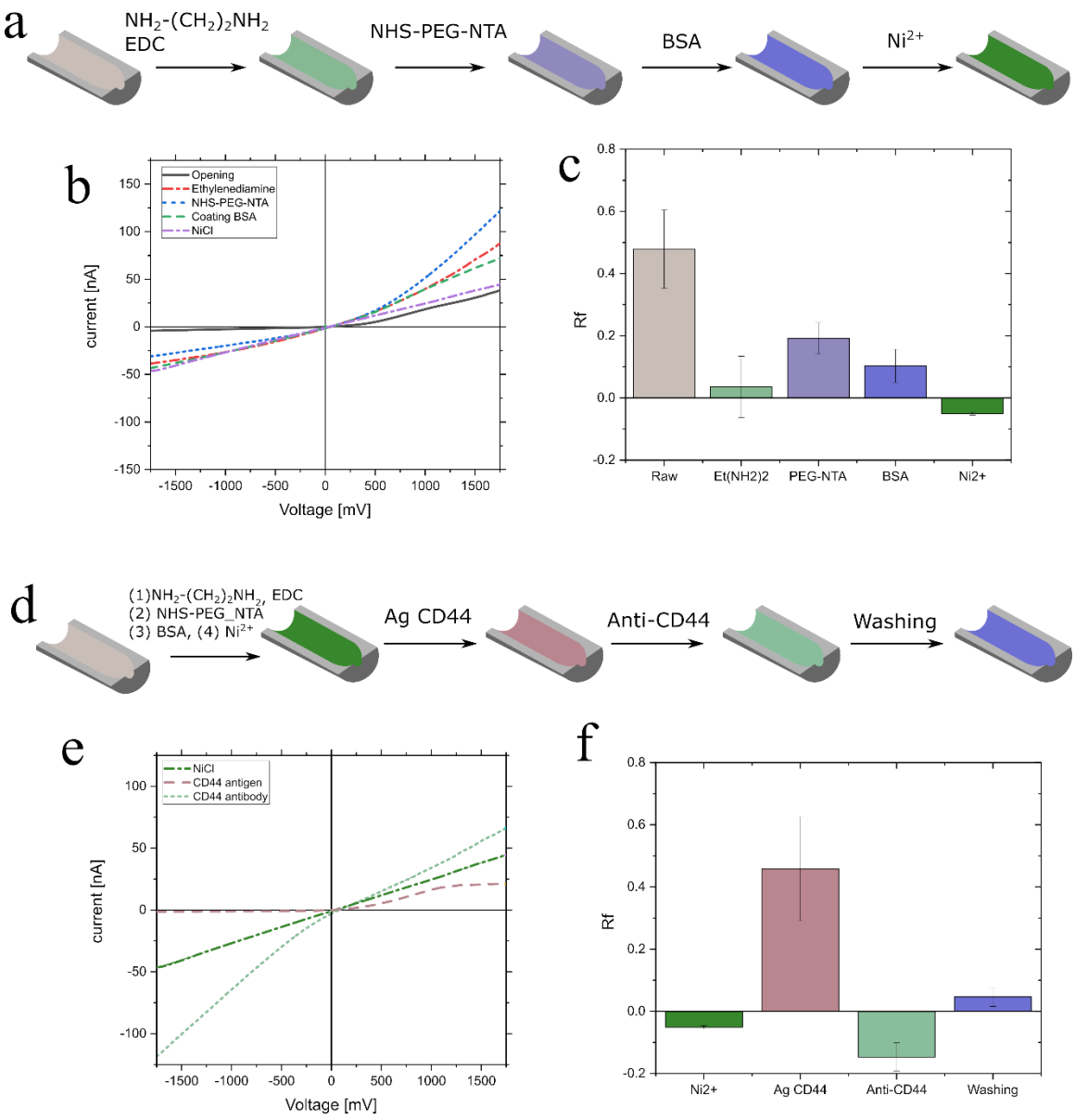

Figure 2 : (a) Illustration of the functionalization steps of the single and multipore nanopore membranes (b) I-V curve obtained after each functionalization steps using PBS 1X (c) histogram of mean R_f value obtained from 8 individual singles nanopores (d_{tip} = 130 +/- 20 nm and D_{base} = 320 +/- 50 nm). (d) Illustration of the detection and elution steps of the single and multipore nanopore membranes (e) I-V curve obtained after each detection and washing steps (f) histogram of mean R_f value obtained from 8 individual singles nanopore. The error bars are the means error obtain from the 8 individual singles nanopore.

At this stage, we have to evaluate the selectivity of the single nanopore against antibodies and other proteins. After 3h incubation with anti-BSA (n=6 independent nanopore), we did not observe any inversion of the rectification factor (figure 3). This means that there is no BSA binding site accessible in the nanopore from the coating. Similar results were obtained using anti-avidin (n=3 independent nanopore). Regardless the antibody, a small variation of R_f may occur due to non-specific interactions or adsorption. Nevertheless, this does not compromise the efficiency of the nanopore sensor. Indeed, after incubation with anti-BSA or anti-avidin, the nanopore remains functional to detect anti-CD44 as shown by the inversion of the current rectification (figure 3).

We have also evaluated whether the addition of different proteins induces a disruption of the R_f due to non-specific adsorption. For this purpose, a series of proteins was incubated in the AgCD44-functionalized nanopore. After washing with PBS, the I-V response remained the same, as the rectification factor (Figure 3e). This means that the selected proteins do not modify the surface properties of the nanopore and therefore their eventual adsorption can be neglected. After incubating these proteins, the nanopore sensor remains functional. However, it should be noted that without an optimal BSA coating, the R_f is modified after protein incubation.

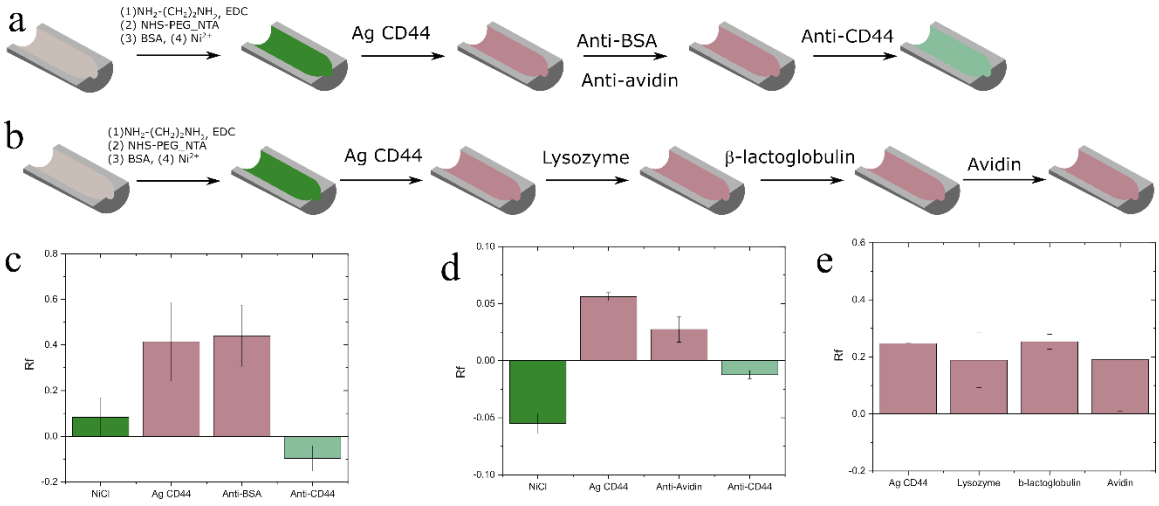

Figure 3 : (a) Illustration of selectivity tests performed for single nanopore membranes against (a) antibodies and (b) proteins (c) histogram of mean R_f value obtained from n individual singles nanopores after incubation with (c) anti-BSA (n=6), (d) anti-avidin (n=3) and (e) various proteins (n=3). The error bars are the means error obtain from the n individual singles nanopore. The nanopore size are d_{tip} = 130 +/- 20 nm and D_{base} = 320 +/- 50 nm.

3.3. Separation by multipore membrane and sensing of eluted anti-CD44 at the single molecule scale

We have previously demonstrated on a single nanopore membrane that functionalization with AgCD44 was efficient in detecting anti-CD44. The washing with imidazole solution suggested that the complex AgCD44/anti-CD44 should be removed from the pore. To verify this and thereby validate our approach to antibody separation, we designed multipore membranes containing cylindrical pores of 100 nm of +/- 20 nm diameter following strictly the same steps as the single nanopore. After grafting the AgCD44, anti-CD44 solutions were filtered before washing with imidazole\EDTA solution. The eluted solution obtained with unlabelled anti-CD44 was analysed by single SiN nanopore of 9.7 nm diameter and 12 nm thickness obtained by dielectric breakdown. In the first step, solutions of AgCD44, anti-CD44 and the complex anti-CD44/AgCD44 were

282 analysed by the nanopore. The current traces show for each sample current blockades that can
283 be assigned to the analyte. The amplitude of the current blockades for AgCD44 and anti-CD44 are
284 centred at 0.03 and 0.04 respectively. This may seem counter-intuitive given the difference in
285 volume of the two proteins (i.e.: 61 nm^3 and 356 nm^3 respectively). We notice, however, that the
286 size of anti-CD44 is larger than the nanopore and therefore only bumping events can be recorded.
287 This is confirmed by a shorter dwell time recorded for the anti-CD44 than the AgCD44 (Figure 4).
288 Conversely, the AgCD44 antigen can translocate into the nanopore. Based on the calculation
289 proposed by Yusko et *al. [69]*, it is possible to obtain a theoretical value for the amplitude of the
290 current blockage by assuming a spheroidal oblate geometry of the AgCD44.

$$\frac{\Delta I}{I_0} = \frac{\Lambda\gamma}{\pi r_p^2\left(l_p + 1.6r_p\right)} S\left(\frac{r_p}{2R_h}\right) \quad (2)$$

291 where Λ is the protein volume, γ is a scaling factor, $S\left(\frac{r_p}{2R_h}\right)$ correction factor that calculates the
292 effective hydrodynamic radius R_h of the protein inside the nanopore (equation 4).

$$S\left(\frac{r_p}{2R_h}\right) = \frac{1}{1 - 0.8\left(\frac{R_h}{r_p}\right)^3} \quad (3)$$

293 In the equation 2, γ dependents on the shape of the protein, for a spherical one it is equal to 1.5.
294 For a spheroid, the value of γ depends on the orientation (parallel ‖ or perpendicular⊥) of the
295 protein relative to the electrical field. Form factors relative to the orientation $\gamma_{\|}$ and $\gamma_{\perp}$are given
296 by equation 5 [69] .

$$\gamma_{\|} = \frac{1}{1 - n_{\|}} \; and \; \gamma_{\perp} = \frac{1}{1 - n_{\perp}} \quad (4)$$

297 Where $n_{\|}$ and $n_{\perp}$are dependent on the ratio m of two hydrodynamic radii. The antibodies have
298 an oblate shape m=a/b. The form is given by the equation 5 and 7

$$n_{\parallel} = \frac{1}{1-m^2}\left[1 - \frac{m}{\sqrt{1-m^2}}\cos^{-1}(m)\right] \quad (5)$$

$$n_{\perp} = \frac{(1-n_{\parallel})}{2} \quad (6)$$

Taking as radius a= 2 nm and b= 2.7 nm (from the PBD structure), the expected $\Delta I/I_0$ (according to a parallel and perpendicular orientations 0.05 and 0.09 respectively) are larger than measured one (centred to 0.03). The experimental values lower than expected could be due to a change in the structure of the protein under the effect of the electric field in the pore [70]. We also observe that the dwell time is ms scale is larger than the theoretical one as previously reported for the experiment conducted at sampling rate of 200 kHz [42,71]. This was assigned to the ability to detect only the protein that interacts with the nanopore [42]. The $\Delta I/I_0$ obtained for the AgCD44/anti-CD44 complex are centred on 0.06 (Figure 4). This shift toward larger values can be attributed to a larger volume of the complex than that of the anti-CD44, thus inducing a larger blocking amplitude during the bump. Interestingly, the dwell time increase regarding the antiCD44 that can be assigned to the larger volume of the complex and thus an increase of the diffusion coefficient.

The eluted solution from the multipore membrane was then analysed by the same single SiN nanopore. To do so, we measured current blockade during 25 min with a frequency rate of 0.11 events/s. Even if this capture rate is low, it confirms that proteins are eluted from the membrane. The analysis of the $\Delta I/I_0$ reveals that the distributions are centred on 0.03. This corresponds well with the expected values for non-complexed anti-CD44 and AgCD44. In addition, the distribution of dwell time is spread suggesting that translocation and bumping are recorded. These results could be explained by the dissociation of AgCD44/anti-CD44 complex during the washing process.

In order to confirm this, filtration experiments with anti-CD44 labelled with alexa fluor 647 were performed. In order to observe a fluorescence signal in the elution product, we used a confocal system to perform fluorescence correlation spectroscopy measurements. First, a fluorescence signal was observed for the filtration product confirming the presence of anti-CD44 in the elution product. Self-correlation function analysis did not reveal a significant increase in the diffusion coefficient of antiCD44 due to its complexation with AgCD44. This is consistent with the nanopore analysis which suggests that the washing with imidazole\EDTA allow the elution of the anti-CD44 and AgCD44 but separates the two entities.

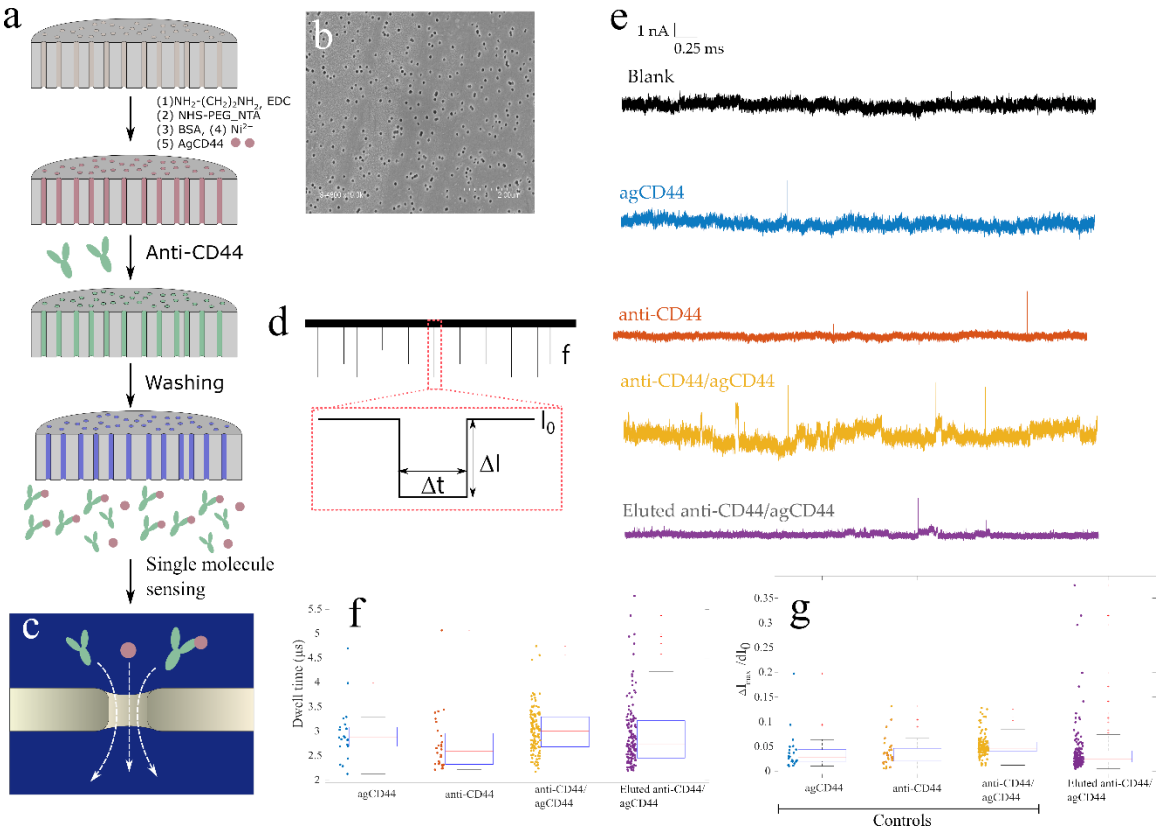

Figure 4 : a. Scheme of the filtration process through a multipore membrane. b. scanning electron microscope image of the multipore membrane, c. Scheme of the detection process by a solid state nanopore, d. Scheme of the resistive pulse showing an event having a current blockade $\Delta I/I_0$ and dwell time Δt, e. Traces of each of the measured proteins (AgCD44 in blue,

anti-CD44 in orange, the complex in yellow) and the eluted solution in violet shown here by the membrane trace, f. Boxplot for the logarithm of the dwell time of all the events obtained from each protein and the filtered membrane solutions, e. boxplots for the current blockade of all the protein and filtered solutions.

4. Conclusion

In summary, we designed single nanopores ionic diode sensors to detect anti-CD44 by a simple I-V curve measurement. The use of a bullet-like shape allows a good reproducibility, despite variability inherent to the individual measurement. The multipore membrane obtained under strictly the same conditions allowed the capture of the antibodies and their analysis by two methods (nanopore and FCS). The elution product contains the uncomplexed antibody. Thus, we show that it is possible to design a membrane based on single and multipore track-etched technique for the separation of antibodies with an associated sensor allowing the parallel detection of the antibody capture from the bulk solution. Next, using SiN nanopore sensors, further analysis on the elution product allows to obtain information on the assembly of the two entities antibody and antigens. We expect that the combination of a multipore membrane with the ionic diode sensor in a microfluidic system could provide a novel versatile nanopore-based device for an unprecedented fast preparation of analytical samples or the production of antibodies. In addition, the parallel detection of traces of a target antibody could allow a pre-control of the sample before a deeper and costly analysis.

Acknowledgments

This work was founded by Agence Nationale de la Recherche (ANR-19-CE42-0006, NanoOligo) and l'institut Carnot Chimie Balard Cirimat (ref16CARN000801). Single tracks have been produced in

GANIL (Caen, France) in the framework of an EMIR project. The authors thank E. Balanzat at CIMAP Caen for support to produce tracked polymer film.

References

[1] J.K. Aronson, R.E. Ferner, Biomarkers-A General Review, Current Protocols in Pharmacology 76 (2017) 9.23.1-9.23.17.

[2] O. Yang, M. Qadan, M. Ierapetritou, Economic Analysis of Batch and Continuous Biopharmaceutical Antibody Production: A Review, J Pharm Innov 14 (2019) 1–19.

[3] S. Liu, Z. Li, B. Yu, S. Wang, Y. Shen, H. Cong, Recent advances on protein separation and purification methods, Advances in Colloid and Interface Science 284 (2020) 102254.

[4] Z. Zhu, J.J. Lu, S. Liu, Protein separation by capillary gel electrophoresis: a review, Analytica Chimica Acta 709 (2012) 21–31.

[5] C.K. Larive, S.M. Lunte, M. Zhong, M.D. Perkins, G.S. Wilson, G. Gokulrangan, T. Williams, F. Afroz, C. Schöneich, T.S. Derrick, C.R. Middaugh, S. Bogdanowich-Knipp, Separation and analysis of peptides and proteins, Anal. Chem. 71 (1999) 389R-423R.

[6] K.K.R. Tetala, M.A. Vijayalakshmi, A review on recent developments for biomolecule separation at analytical scale using microfluidic devices, Analytica Chimica Acta 906 (2016) 7–21.

[7] M. Sonker, V. Sahore, A.T. Woolley, Recent advances in microfluidic sample preparation and separation techniques for molecular biomarker analysis: A critical review, Analytica Chimica Acta 986 (2017) 1–11.

[8] H.J. Issaq, The role of separation science in proteomics research, Electrophoresis 22 (2001) 3629–3638.

[9] R. Ghosh, Protein separation using membrane chromatography: opportunities and challenges, Journal of Chromatography A 952 (2002) 13–27.

[10] S. AHMED, A. LUTES, T. BARBARI, Specific capture of target proteins by oriented antibodies bound to tyrosinase-immobilized Protein A on a polyallylamine affinity membrane surface, Journal of Membrane Science 282 (2006) 311–321.

[11] D. YU, M. MCLEAN, J. HALL, R. GHOSH, Purification of monoclonal antibody from tobacco extract using membrane-based bioseparation techniques, Journal of Membrane Science 323 (2008) 159–166.

[12] L. Wang, R. Ghosh, Fractionation of monoclonal antibody aggregates using membrane chromatography, Journal of Membrane Science 318 (2008) 311–316.

[13] J. Wang, E.W. Jenkins, J.R. Robinson, A. Wilson, S.M. Husson, A new multimodal membrane adsorber for monoclonal antibody purifications, Journal of Membrane Science 492 (2015) 137–146.

[14] A.L. Zydney, New developments in membranes for bioprocessing – A review, Journal of Membrane Science 620 (2021) 118804.

[15] E. Klein, Affinity membranes: a 10-year review, Journal of Membrane Science 179 (2000) 1–27.

[16] G. Brisson, M. Britten, Y. Pouliot, Electrically-enhanced crossflow microfiltration for separation of lactoferrin from whey protein mixtures, Journal of Membrane Science 297 (2007) 206–216.
[17] N. Meyer, I. Abrao-Nemeir, J.-M. Janot, J. Torrent, M. Lepoitevin, S. Balme, Solid-state and polymer nanopores for protein sensing: A review, Advances in Colloid and Interface Science 298 (2021) 102561.
[18] P.Y. Apel, I.V. Blonskaya, O.L. Orelovitch, S.N. Dmitriev, Diode-like ion-track asymmetric nanopores: Some alternative methods of fabrication, Nuclear Instruments and Methods in Physics Research Section B: Beam Interactions with Materials and Atoms 267 (2009) 1023–1027.
[19] P.Y. Apel, I.V. Blonskaya, O.L. Orelovitch, P. Ramirez, B.A. Sartowska, Effect of nanopore geometry on ion current rectification, Nanotechnology 22 (2011) 175302.
[20] K.-J. Kim, P.V. Stevens, A.G. Fane, Porosity dependence of pore entry shape in track-etched membranes by image analysis, Journal of Membrane Science 93 (1994) 79–90.
[21] V. Chavan, C. Agarwal, A.K. Pandey, J.P. Nair, P. Surendran, P.C. Kalsi, A. Goswami, Controlled development of pores in polyethylene terepthalate sheet by room temperature chemical etching method, Journal of Membrane Science 471 (2014) 185–191.
[22] S. Dutt, P. Apel, N. Lizunov, C. Notthoff, Q. Wen, C. Trautmann, P. Mota-Santiago, N. Kirby, P. Kluth, Shape of nanopores in track-etched polycarbonate membranes, Journal of Membrane Science 638 (2021) 119681.
[23] T. Ma, J.-M. Janot, S. Balme, Track-Etched Nanopore/Membrane: From Fundamental to Applications, Small Methods 4 (2020) 2000366.
[24] I.V. Blonskaya, N.E. Lizunov, K. Olejniczak, O.L. Orelovich, Y. Yamauchi, M.E. Toimil-Molares, C. Trautmann, P.Y. Apel, Elucidating the roles of diffusion and osmotic flow in controlling the geometry of nanochannels in asymmetric track-etched membranes, Journal of Membrane Science 618 (2021) 118657.
[25] Z.S. Siwy, Ion-Current Rectification in Nanopores and Nanotubes with Broken Symmetry, Adv. Funct. Mater. 16 (2006) 735–746.
[26] Z. Siwy, E. Heins, C.C. Harrell, P. Kohli, C.R. Martin, Conical-Nanotube Ion-Current Rectifiers: The Role of Surface Charge, J. Am. Chem. Soc. 126 (2004) 10850–10851.
[27] M. Ali, B. Yameen, J. Cervera, P. Ramírez, R. Neumann, W. Ensinger, W. Knoll, O. Azzaroni, Layer-by-layer assembly of polyelectrolytes into ionic current rectifying solid-state nanopores: insights from theory and experiment, J. Am. Chem. Soc. 132 (2010) 8338–8348.
[28] G. Laucirica, Y.T. Terrones, V. Cayón, M.L. Cortez, M.E. Toimil-Molares, C. Trautmann, W. Marmisollé, O. Azzaroni, Biomimetic Solid-State Nanochannels for Chemical and Biological Sensing Applications, TrAC Trends in Analytical Chemistry (2021) 116425.
[29] M. Ali, S. Nasir, W. Ensinger, Bioconjugation-induced ionic current rectification in aptamer-modified single cylindrical nanopores, Chemical communications (Cambridge, England) 51 (2015) 3454–3457.

[30] M. Ali, P. Ramirez, M.N. Tahir, S. Mafe, Z. Siwy, R. Neumann, W. Tremel, W. Ensinger, Biomolecular conjugation inside synthetic polymer nanopores via glycoprotein-lectin interactions, Nanoscale 3 (2011) 1894–1903.
[31] M. Ali, M.N. Tahir, Z. Siwy, R. Neumann, W. Tremel, W. Ensinger, Hydrogen peroxide sensing with horseradish peroxidase-modified polymer single conical nanochannels, Analytical chemistry 83 (2011) 1673–1680.
[32] M.N. Tahir, M. Ali, R. Andre, W.E.G. Müller, H.-C. Schröder, W. Tremel, W. Ensinger, Silicatein conjugation inside nanoconfined geometries through immobilized NTA-Ni(II) chelates, Chem. Commun. 49 (2013) 2210–2212.
[33] M. Lepoitevin, M. Bechelany, E. Balanzat, J.-M. Janot, S. Balme, Non-Fluorescence label protein sensing with track-etched nanopore decorated by avidin/biotin system, Electrochimica Acta 211 (2016) 611–618.
[34] M. Lepoitevin, B. Jamilloux, M. Bechelany, E. Balanzat, J.-M. Janot, S. Balme, Fast and reversible functionalization of a single nanopore based on layer-by-layer polyelectrolyte self-assembly for tuning current rectification and designing sensors, RSC advances 6 (2016) 32228–32233.
[35] I. Duznovic, A. Gräwe, W. Weber, L.K. Müller, M. Ali, W. Ensinger, A. Tietze, V. Stein, Ultrasensitive and Selective Protein Recognition with Nanobody-Functionalized Synthetic Nanopores, Small (Weinheim an der Bergstrasse, Germany) 17 (2021) e2101066.
[36] T. Ma, E. Balanzat, J.-M. Janot, S. Balme, Single conical track-etched nanopore for a free-label detection of OSCS contaminants in heparin, Biosensors & bioelectronics 137 (2019) 207–212.
[37] J. Li, D. Stein, C. McMullan, D. Branton, M.J. Aziz, J.A. Golovchenko, Ion-beam sculpting at nanometre length scales, Nature 412 (2001) 166–169.
[38] L. Xue, H. Yamazaki, R. Ren, M. Wanunu, A.P. Ivanov, J.B. Edel, Solid-state nanopore sensors, Nat Rev Mater 5 (2020) 931–951.
[39] R. Hu, J.V. Rodrigues, P. Waduge, H. Yamazaki, B. Cressiot, Y. Chishti, L. Makowski, D. Yu, E. Shakhnovich, Q. Zhao, M. Wanunu, Differential Enzyme Flexibility Probed Using Solid-State Nanopores, ACS nano 12 (2018) 4494–4502.
[40] J. Larkin, R.Y. Henley, M. Muthukumar, J.K. Rosenstein, M. Wanunu, High-bandwidth protein analysis using solid-state nanopores, Biophysical Journal 106 (2014) 696–704.
[41] P. Waduge, R. Hu, P. Bandarkar, H. Yamazaki, B. Cressiot, Q. Zhao, P.C. Whitford, M. Wanunu, Nanopore-Based Measurements of Protein Size, Fluctuations, and Conformational Changes, ACS nano 11 (2017) 5706–5716.
[42] S. Balme, P.E. Coulon, M. Lepoitevin, B. Charlot, N. Yandrapalli, C. Favard, D. Muriaux, M. Bechelany, J.-M. Janot, Influence of Adsorption on Proteins and Amyloid Detection by Silicon Nitride Nanopore, Langmuir 32 (2016) 8916–8925.
[43] L. Reynaud, A. Bouchet-Spinelli, J.-M. Janot, A. Buhot, S. Balme, C. Raillon, Discrimination of α-Thrombin and γ-Thrombin Using Aptamer-Functionalized Nanopore Sensing, Anal. Chem. 93 (2021) 7889–7897.
[44] E.C. Yusko, B.R. Bruhn, O.M. Eggenberger, J. Houghtaling, R.C. Rollings, N.C. Walsh, S. Nandivada, M. Pindrus, A.R. Hall, D. Sept, J. Li, D.S. Kalonia, M. Mayer, Real-time shape approximation and fingerprinting of single proteins using a nanopore, Nature Nanotech 12 (2017) 360–367.

[45] E.C. Yusko, P. Prangkio, D. Sept, R.C. Rollings, J. Li, M. Mayer, Single-Particle Characterization of Aβ Oligomers in Solution, ACS nano 6 (2012) 5909–5919.
[46] H. Chae, D.-K. Kwak, M.-K. Lee, S.-W. Chi, K.-B. Kim, Solid-state nanopore analysis on conformation change of p53TAD-MDM2 fusion protein induced by protein-protein interaction, Nanoscale 10 (2018) 17227–17235.
[47] J. Li, D. Fologea, R. Rollings, B. Ledden, Characterization of Protein Unfolding with Solid-state Nanopores, PPL 21 (2014) 256–265.
[48] M. Firnkes, D. Pedone, J. Knezevic, M. Döblinger, U. Rant, Electrically facilitated translocations of proteins through silicon nitride nanopores: conjoint and competitive action of diffusion, electrophoresis, and electroosmosis, Nano letters 10 (2010) 2162–2167.
[49] D. Fologea, B. Ledden, D.S. McNabb, J. Li, Electrical characterization of protein molecules by a solid-state nanopore, Applied physics letters 91 (2007) 539011–539013.
[50] J. Houghtaling, C. Ying, O.M. Eggenberger, A. Fennouri, S. Nandivada, M. Acharjee, J. Li, A.R. Hall, M. Mayer, Estimation of Shape, Volume, and Dipole Moment of Individual Proteins Freely Transiting a Synthetic Nanopore, ACS nano 13 (2019) 5231–5242.
[51] L. Reynaud, A. Bouchet-Spinelli, C. Raillon, A. Buhot, Sensing with Nanopores and Aptamers: A Way Forward, Sensors (Basel, Switzerland) 20 (2020).
[52] Y.-L. Ying, R.-J. Yu, Y.-X. Hu, R. Gao, Y.-T. Long, Single antibody-antigen interactions monitored via transient ionic current recording using nanopore sensors, Chem. Commun. 53 (2017) 8620–8623.
[53] M. Waugh, K. Briggs, D. Gunn, M. Gibeault, S. King, Q. Ingram, A.M. Jimenez, S. Berryman, D. Lomovtsev, L. Andrzejewski, V. Tabard-Cossa, Solid-state nanopore fabrication by automated controlled breakdown, Nat Protoc 15 (2020) 122–143.
[54] H. Kwok, K. Briggs, V. Tabard-Cossa, Nanopore fabrication by controlled dielectric breakdown, PloS one 9 (2014) e92880.
[55] S. Balme, T. Ma, E. Balanzat, J.-M. Janot, Large osmotic energy harvesting from functionalized conical nanopore suitable for membrane applications, Journal of Membrane Science 544 (2017) 18–24.
[56] T. Ma, E. Balanzat, J.-M. Janot, S. Balme, Nanopore Functionalized by Highly Charged Hydrogels for Osmotic Energy Harvesting, ACS Appl. Mater. Interfaces 11 (2019) 12578–12585.
[57] M. Lepoitevin, T. Ma, M. Bechelany, J.-M. Janot, S. Balme, Functionalization of single solid state nanopores to mimic biological ion channels: A review, Advances in Colloid and Interface Science 250 (2017) 195–213.
[58] H. Xu, M. Niu, X. Yuan, K. Wu, A. Liu, CD44 as a tumor biomarker and therapeutic target, Exp Hematol Oncol 9 (2020) 36.
[59] H.A. Runnels, G.L. Weber, J. Min, E.M. Kudlacz, J.F. Zobel, C.B. Donovan, M.A. Thiede, J. Zhang, R.B. Alpert, M.A. Salafia, A.J. Milici, D. Burdette, R.R. Bell, J.S. Beebe, X. Xu, PF-03475952: a potent and neutralizing fully human anti-CD44 antibody for therapeutic applications in inflammatory diseases, Adv Therapy 27 (2010) 168–180.

[60] P.Y. Apel, I.V. Blonskaya, S.N. Dmitriev, O.L. Orelovitch, A. Presz, B.A. Sartowska, Fabrication of nanopores in polymer foils with surfactant-controlled longitudinal profiles, Nanotechnology 18 (2007) 305302.
[61] P.Y. Apel, I.V. Blonskaya, N.E. Lizunov, K. Olejniczak, O.L. Orelovitch, M.E. Toimil-Molares, C. Trautmann, Osmotic Effects in Track-Etched Nanopores, Small (Weinheim an der Bergstrasse, Germany) 14 (2018) e1703327.
[62] S. SIRIJARUKUL, E. BALANZAT, E. VASINA, P. DEJARDIN, Flat sheet membrane with controlled variation of pore density and pore size in a direction parallel to the surface☆, Journal of Membrane Science 296 (2007) 185–194.
[63] K. Kececi, L.T. Sexton, F. Buyukserin, C.R. Martin, Resistive-pulse detection of short dsDNAs using a chemically functionalized conical nanopore sensor, Nanomedicine (London, England) 3 (2008) 787–796.
[64] P.Y. Apel, I.V. Blonskaya, S.N. Dmitriev, O.L. Orelovich, B.A. Sartowska, Ion track symmetric and asymmetric nanopores in polyethylene terephthalate foils for versatile applications, Nuclear Instruments and Methods in Physics Research Section B: Beam Interactions with Materials and Atoms 365 (2015) 409–413.
[65] Z.J. Grzywna, Z. Siwy, C.L. Bashford, Nonlinear theory for ionic transport through track-etched nuclear membranes, Journal of Membrane Science 121 (1996) 261–269.
[66] D.Y. Butylskii, N.D. Pismenskaya, P.Y. Apel, K.G. Sabbatovskiy, V.V. Nikonenko, Highly selective separation of singly charged cations by countercurrent electromigration with a track-etched membrane, Journal of Membrane Science 635 (2021) 119449.
[67] T. Ma, N. Arroyo, J. Marc Janot, F. Picaud, S. Balme, Conformation of Polyethylene Glycol inside Confined Space: Simulation and Experimental Approaches, Nanomaterials (Basel, Switzerland) 11 (2021).
[68] D. Coglitore, J.-M. Janot, S. Balme, Protein at liquid solid interfaces: Toward a new paradigm to change the approach to design hybrid protein/solid-state materials, Advances in Colloid and Interface Science 270 (2019) 278–292.
[69] E.C. Yusko, J.M. Johnson, S. Majd, P. Prangkio, R.C. Rollings, J. Li, J. Yang, M. Mayer, Controlling protein translocation through nanopores with bio-inspired fluid walls, Nature Nanotech 6 (2011) 253–260.
[70] A. Carlsen, V. Tabard-Cossa, Mapping shifts in nanopore signal to changes in protein and protein-DNA conformation, Proteomics (2021) e2100068.
[71] C. Plesa, S.W. Kowalczyk, R. Zinsmeester, A.Y. Grosberg, Y. Rabin, C. Dekker, Fast translocation of proteins through solid state nanopores, Nano letters 13 (2013) 658–663.